Chinese Chemical Letters 34 (2023) 107389

Contents lists available at ScienceDirect

Chinese Chemical Letters

journal homepage: www.elsevier.com/locate/cclet

# Renewable wood-derived hierarchical porous, N-doped carbon sheet as a robust self-supporting cathodic electrode for zinc-air batteries

Xiaohua Deng[a], Zhu Jiang[a], Yingying Chen[a], Dai Dang[a,*], Quanbing Liu[a], Xiaoyang Wang[b,*], Xu Yang[a]

[a] School of Chemical Engineering and Light Industry, Guangdong University of Technology, Guangzhou 510006, China
[b] Department of Chemical Systems Engineering, Graduate School of Engineering, Nagoya University, Furo-cho, Chikusa-ku, Nagoya 464-8603, Japan

ARTICLE INFO

*Article history:*
Received 20 January 2022
Revised 19 February 2022
Accepted 30 March 2022
Available online 2 April 2022

*Keywords:*
Carbon sheet
Hierarchical porous structure
Metal-free
Zinc-air batteries
Long-life stability

ABSTRACT

Heteroatom doped porous carbon materials have emerged as essential cathode material for metal-air battery systems in the context of soaring demands for clean energy conversion and storage. Herein, a three-dimensional nitrogen-doped carbon self-supported electrode (TNCSE) is fabricated through thermal treatment and acid activation of raw wood. The resulting TNCSE retains the hierarchical porous architecture of parent raw lumber and holds substantial defect sites and doped N sites in the carbon skeleton. Assembled as a cathode in the rechargeable zinc-air battery, the TNCSE exhibits a superior peak power density of 134.02 mW/cm$^2$ and an energy density of 835.92 mAh/g, significantly exceeding the ones reference commercial 20% Pt/C does. More strikingly, a limited performance decay of 1.47% after an ultra long-period (500 h) cycle is also achieved on the TNCSE. This work could offer a green and cost-save approach for rationally converting biomass into a robust self-supporting cathode material for a rechargeable zinc-air battery.

© 2022 Published by Elsevier B.V. on behalf of Chinese Chemical Society and Institute of Materia Medica, Chinese Academy of Medical Sciences.

Rechargeable zinc-air battery (ZAB), as a new type of energy storage device, has earned much attention from numerous researchers, owing to its advantages of low cost, high safety, sound theoretical specific energy, and stable discharge potential (1.2-1.4 V), and so on. Similar to other general metal-air batteries, the overall performances of ZAB are limited by their cathodic reversible oxygen reduction/evolution reactions (ORR/OER) as they underwent the discharging/charging process, which frequently comes up with undesirable electrochemical activity and slow mass transfer at the gas-liquid-solid three-phase interface [1–5].

To resolve the above low electrocatalytic issues, much effort has been dedicated to designing metal-containing or metal-free cathode catalysts with high efficiency, sun as transition metal compounds [6–12], transition metal single atoms [13–17], carbon-based materials [18–21], and chalcogenides [22]. Amongst these metal-free catalysts, heteroatom-doped hierarchical carbons have evoked researchers' great interest because of their multi-functional properties. Albeit the pristine carbon hardly stimulates the ORR/OER reactions due to the lack of electrochemically active sites, heteroatom-doping could afford such centers. For example, doping carbon with nitrogen enables the fast electro-absorption of the adjacent carbon atoms at the N doping site due to the increased electronegativity of N (3.04) above C (2.55) [23–25]. As a result, altering the electronic structure between N and C atoms will improve $O_2$ and $OH^-$ adsorption behavior and facilitate intermediate reactions' transfer under electrostatic forces. Besides, the carbon itself could serve as a conductive carrier to smooth electron transportation, and the hierarchical pores within the carbon matrix could accommodate the active sites and promote mass transfer.

Apart from the electrochemical activity, the sluggish and complicated mass transfer at the triple-phase interface of the air cathode is another critical factor that affects the ZAB performance. As depicted in Fig. 1, The conventional air cathode is typically prepared with a carbon paper or carbon cloth loaded with catalyst by stacking carbon fibers, in which the catalyst mainly adheres to the carbon paper through a hydrophobic binder (*e.g.*, PTFE) [26]. However, the non-conductive binder restricts the accessibility of active sites, and the disordered micro-pores hardly offer continuous and efficient channels for gases, electrolytes, and electrons [27–29]. During the period of discharge, the $Zn^{2+}$ ions gradually react with oxygen to form an insoluble solid ZnO product in the air cathode accumulating inside the pore structure at triple-phase sites, which would be continued block the accesses for oxygen and forbid the $Zn^{2+}$ diffusion to the active sites, and eventually reduces

* Corresponding authors.
*E-mail addresses:* dangdai@gdut.edu.cn (D. Dang), wxy@sp.material.nagoya-u.ac.jp (X. Wang).

https://doi.org/10.1016/j.cclet.2022.03.112
1001-8417/© 2022 Published by Elsevier B.V. on behalf of Chinese Chemical Society and Institute of Materia Medica, Chinese Academy of Medical Sciences.

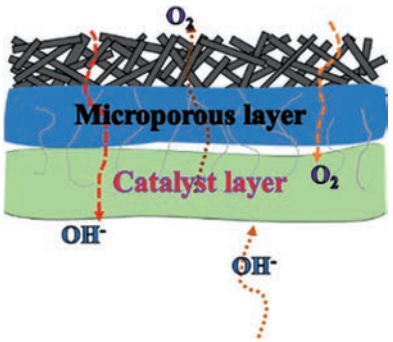


**Fig. 1.** Schematic diagram of the conventional microstructure of air cathode.

the active area of the cathode [29]. Therefore, the desired cathode structure having an open hierarchical porous structure with interconnected macropores can promote gas and ion diffusion and many micro-pores containing the by-products during the discharge process [30–32]. Conventional self-supporting carbon composites, such as carbon paper, carbon nanofibers, and carbon cloth used in air cathodes are costly and complicated in fabrication processes, unfavorable for the commercialization of ZAB. Other powder catalysts require a binder to load them onto self-supporting carbon cloth/paper when preparing air cathodes, in which the binder prevents gas permeability, covers the active sites, and reduces the performance of ZAB [33,34].

Therefore, creating an inexpensive three-dimensional air electrode with a facile manufacturing process and a hierarchical porous structure for practical ZAB implementation is urgently desirable. As a renewable resource on earth, wood has a natural hierarchical pore structure, including nanoscale, micron-scale, and macroscale pore features. Low curvature channels will form a hierarchical interconnected porous structure after activation treatment [35,36]. In addition, the natural 3D oriented microchannel structure can shorten the ion/active species transport routes to accelerate kinetic processes and facilitate the diffusion of gas and electrolytes [37–39].

Herein, as the continuation of our previous work [26] and inspired by the unique attributions of natural wood (3D hierarchical porous, rigid strength, and fine microchannels), we have prepared an N-doped self-supporting carbon electrode with a high capacity of hierarchical 3D connected porosity *via in situ* carbonizations of the naturally renewable pine logs. The resulting 3D N-doped carbon self-supported electrode (TNCSE) not only retained their architecture of parent raw lumber but also held enriched surface defect sites and N-doped sites within the carbon frame, both of which serve as the essential active centers for electrocatalysis. A superior high specific capacity and energy density of 772.07 mAh/g and 835.92 mAh/g were accomplished over the TNCSE, significantly exceeding the ones reference commercial 20% Pt/C did. Furthermore, a slight degradation of 1.47% after 500 h cycles demonstrated its robust stability. The TNCSE shed light on developing high-performance carbon cathodes for ZAB *via* a green and low-cost strategy.

Natural pine chips, polytetrafluoroethylene emulsion (PTFE) (6 wt%), Nafion (5%), $HNO_3$ (AR, 65%), $C_2H_5OH$ (AR, 99%), acetone (AR, 99%), isopropyl alcohol (AR, 99%) KOH (AR, 99%), Commercial Pt/C catalyst (JM, 20 wt%), carbon paper (TCP-H-060, Toray, Japan), all chemicals used without further purification.

Natural pine wood was cut vertically in the direction of growth to a thickness of approximately 0.5 cm and dried in an oven at 80 °C for 24 h.

Preparation of carbonized wood (CW): Firstly, the pretreated pine chips were calcined in a muffle furnace at 240 °C for 10 h. After that, the resulting carbonized wood chips were transferred to a tube furnace under Ar atmosphere and pyrolyzed at 1000 °C for 2 h, and the products were collected to obtain CW.

Preparation of three-dimensional nitrogen-doped carbon self-supported electrode (TNCSE): The obtained carbonized wood was polished to a thin slice (2 cm × 2 cm × 2 mm). The piece treated concentrated nitric acid at 80 °C for 0.5 h. Finally, the 3D vertical nitrogen-doped carbon catalysts were obtained by calcination at 900 °C for 2 h in an argon atmosphere, labeled as TNCSE.

The morphologies and structures of the catalysts were recorded with scanning electron microscopy (SEM, SU8220 Hitachi High-Tech). Energy-dispersive X-ray elemental spectroscopy (EDS) and SEM were done on the same machine (SEM, SU8220 Hitachi High-Tech). The phase characteristics of samples were measured on X-ray diffraction (XRD, Dandong Tongda Science & Technology) with a Cu K$\alpha$ radiation ($\lambda = 1.5406$ Å). Raman spectra were performed on UV Laser Raman Spectroscopy (HORIBA) with an excitation wavelength of 633 nm.

The typical three-electrode system was employed on the Ivium Station workstation to perform the electrochemical tests with 1 mol/L KOH aqueous solution (pH 14) as the electrolyte, graphite rod as the counter electrode (CE), Hg/HgO as the reference electrode (RE). The obtained self-supported CW and TNCSE samples could be directly used as the working electrode. For the Powder TNCSE sample, 20 mg of catalysts was dispersed with 1 mL of isopropanol and 20 μL of 5% Nafion mixture and sonicated 0.5 h to form a uniform slurry. 20 μL of the slurry was applied dropwise on carbon paper. The final mass load of the catalyst on the electrode was about 2 mg/cm$^2$. The linear sweep voltammetry (LSV) was carried out with a scan rate of 10 mV/s. The corresponding Tafel curves were based on the Tafel equation ($\eta = b\log|j| + a$, $b$ is the Tafel slope, $j$ is the current density, and $a$ is the intercept). Calculate the potential corresponding to the reversible hydrogen electrode (RHE) electrode by the following formula:

$$E_{RHE} = E_{Ag/AgCl} + (0.197 + 0.059 \times pH) \quad (1)$$

The following formula calculated the overpotential ($\eta$):

$$\eta = E_{RHE} - 1.23 \quad (2)$$

Rechargeable zinc-air cells assembled into a two-electrode structure and made into a two-electrode system. A polished zinc foil was used as the anode of ZAB. The cathode was composed of a piece of intact TNCSE electrode. For hydrophobic treatment, 18 μL of PTFE solution (6 wt%) was dissolved in 1 mL of deionized water and sonicated for 30 min to form a homogeneous suspension. Next, the mixed suspension was evenly sprayed on the outer side of the TNCSE fronting the air. Lastly, the TNCSE was heated up to 350 °C in air and calcined for 30 min at a rate of 5 °C/min.

In comparison with the self-supported TNCSE electrode, powder material was loaded onto carbon paper to make an air cathode: Firstly, the commercial carbon paper was cut into 2 cm × 2 cm. Secondly, 4 mg of the catalyst (20% Pt/C or powder derived from TNCSE was dissolved in 1 mL of ethanol, then dropped into 11 μL of PTFE solution (6 wt%), and sonicated for 30 min to form a uniform suspension. Then, the catalyst suspension was uniformly sprayed on the side of the carbon paper. After the catalyst solvent evaporates, the obtained electrode can be prepared for Zn-air battery assembly and further testing.

The air cathode's exposed area (to electrolyte and air) was 1 cm$^2$. The electrolyte was a 6 mol/L KOH solution to ensure a reversible electrochemical reaction of zinc on the Zn anode.

All ZAB tests were performed at room temperature on the Ivium Station workstation. Each charge and discharge cycle were 20 min, and the current density was 5 mA/cm$^2$. LSV was carried out to record the charge and discharge polarization curve on the Ivium Station workstation, and the scan rate was fixed at 10 mV/s.

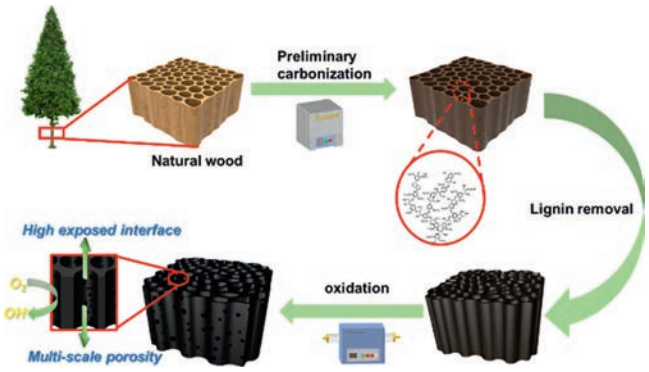


**Fig. 2.** Schematic diagram of the synthesis of TNCSE.

The discharge characteristic curve was obtained by testing at a current density of 20 mA/cm$^2$. Both current density and power density were normalized to the effective surface area of the air electrode.

Battery specific energy calculation formula:

$$\text{specific capacity} = \frac{\text{current} \times \text{service hour}}{\text{weight of consumed zinc}} \quad (3)$$

Energy density calculation formula:

$$\text{energy density} = \frac{\text{current} \times \text{service hour} \times \text{arrage discharge voltage}}{\text{weight of consumed zinc}} \quad (4)$$

By varying the current density (from 1 mA/cm$^2$ to 20 mA/cm$^2$) for a constant current discharge test, the discharge stability of the ZAB can be observed. Then, the discharge multiplier performance and reversibility of the ZAB were determined by adjusting the current density from 20 mA/cm$^2$ to 1 mA/cm$^2$.

With its rigidity, breathability, and outstanding thermal conductivity, the natural wood of pine has been widely used as a raw material in the architecture and furniture industries since ancient times. The preparation process of the TNCSE is shown in Fig. 2. Firstly, to maintain the anisotropic structure of the natural pine wood, the pine chips were obtained by cutting perpendicular to the growth direction of the tree. Then, lignin in the natural wood was removed by thermal treatment, which increased the porosity and maintained the structural integrity of the well-aligned elongated microchannels. The obtained carbon sheet with the physical strength was subjected to the activation of concentrated nitric acid pretreatment, which created defective sites on the surface of the pore walls and immobilized the N source within the hierarchical porous structure. Finally, a self-supported TNCSE air cathode was obtained by further carbonization in $N_2$. TNCSE is an outstanding 3D collector for fast electron transport and mass transfer. In addition, well-aligned microchannels dramatically enhance the penetration of oxygen and shorten the gas diffusion distances, which substantially improve the electrochemical properties of the ZAB.

In Fig. 3a, the TNCSE has a size of 200 mm × 200 mm × 2 mm, preserving the wood's original growth texture and 3D structure. The scanning electron microscope (SEM) images in Fig. 3b shows the multi-porous channel structure of TNCSE. After carbonization and activation, the overall structure of the wood can be preserved perfectly (Fig. S1 in Supporting information), with many vertical upward long channels distributed in the orderly direction of growth and many micropores/mesopores in the straight channels. Fig. 3c illustrates the numerous shallow nanopores found in the microchannel walls of the TNCSE, indicating that the carbon sheet is highly activated. The inset graph and Table S1 (Supporting information) display the uniform distribution of N as a dopant on the carbon skeleton during the activation process. The

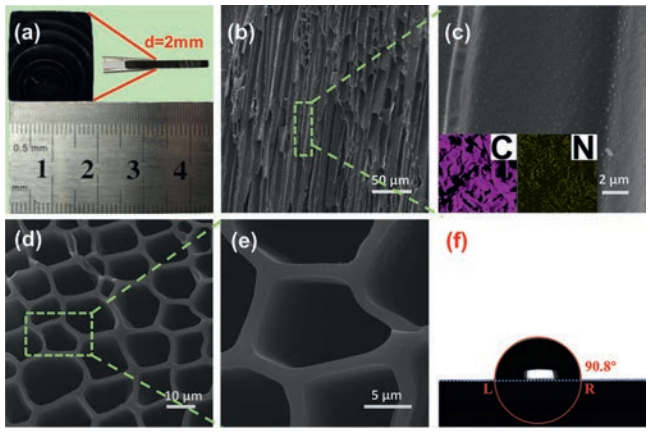


**Fig. 3.** Structure characterizations of TNCSE. (a) Digital photograph demonstrating self-supported TNCSE. (b, c) Scanning electron microscope (SEM) image revealing the well-arranged and well-defined elongated microchannels in the cross-section of TNCSE; inset of (c) elemental mapping diagram indicating the uniform distribution of N elements on TNCSE. (d, e) SEM image illustrating the top view and exposing the remarkably high porosity of TNCSE. (f) A digital photograph depicts the contact angle. The electrolyte droplets diffuse on the cathode surface and immediately penetrate the microchannels.

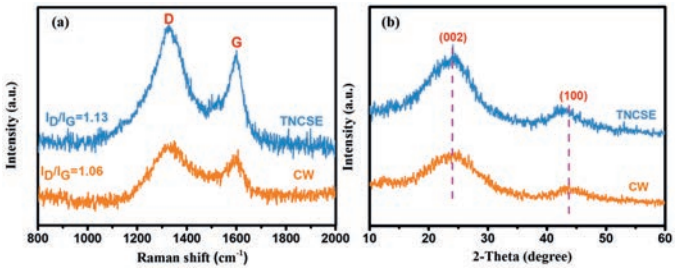


**Fig. 4.** (a) Raman spectra and (b) XRD of TNCSE and CW.

three-dimensional anisotropic structure of TNCSE is well maintained (Figs. 3d and e). The pore channels are parallel to each other in the vertical direction and the vertical cross-section. The cross-section of TNCSE has a highly oriented macropore structure with 5-15 μm in diameter and a smooth surface. After carbonization and activation, the 3D porous framework with initially aligned microchannels of TNCSE has been kept ideally. In addition, the concave and low curvature of the microchannels significantly facilitate the diffusion of oxygen and shorten the diffusion distance. The unique anisotropic structure can achieve higher specific area capacities with an ultra-thick electrode structure. To further evaluate the hydrophilic feature and wettability of TNCSE to the electrolyte, the TNCSE is subjected to contact angle measurements. As shown in Fig. 3f, the contact angle between the TNCSE surface and the electrolyte droplets is 90.8°, while the contact angle of CW without the activation treatment is 123.3° (Fig. S2 in Supporting information), indicating that the surface of the carbon skeleton of TNCSE can generate a lot of hydrophilic groups after the activation treatment, which can make an excellent electrolyte wettability of the cathode, contributing to the enhancement of battery performance. During the reaction, the electrolyte is conveniently absorbed by the cathode and distributed well on the porous walls of the aligned microchannels. Moreover, the pits on the surface of channels acted as a mass exchange pathway between each channel. Their exchangeability allows the migration of ions through the channels to create a thin and continuous ion transport layer without blocking oxygen penetration.

Fig. 4a exhibits the Raman spectrum of the TNCSE. There are two characteristic peaks at 1300 and 1590 cm$^{-1}$, representing

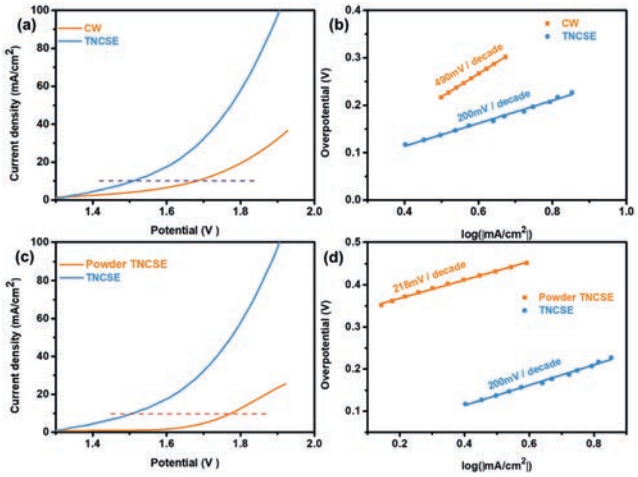


**Fig. 5.** (a, c) Curves of linear sweep voltammetry experiments of CW and TNCSE, Powder TNCSE and TNCSE in 1 mol/L KOH electrolyte for OER. (b, d) Tafel plots of CW and TNCSE, Powder TNCSE and TNCSE.

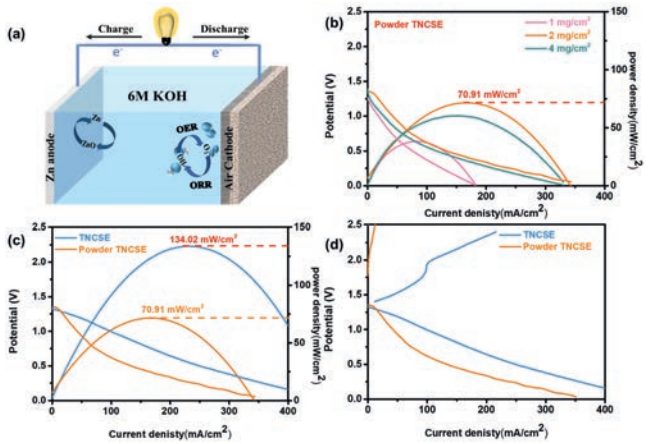


**Fig. 6.** (a) Schematic diagram of rechargeable ZAB. (b) The discharge and power density plots of ZAB were assembled with different powder TNCSE. (c, d) Power density graphs and charge-discharge polarization graphs of ZAB created with TNCSE and powder TNCSE.

D-band and G-band, respectively. The D-band suggests the defective sites due to sheet fracture at the edges of the material, and the G-band represents $sp^2$ bonds in the plane of the carbon material [40]. The $I_D/I_G = 1.06$ ratio of CW without acid activation is lower than that of TNCSE ($I_D/I_G = 1.13$), which indicates that the activation had increased the number of defect sites on the pore wall. On the other hand, the thermal treatment of the carbon sheet has removed more oxygen-containing groups, which has caused the $sp^2$ bonds in the graphene layer to break into $sp^3$ bonds, resulting in more void defects on the surface. Fig. 4b demonstrates the crystal structures of CW and TNCSE analyzed by X-ray diffraction (XRD). After carbonization, broader $2\theta$ peaks at 23.8° and 44° appear, corresponding to the (002) and (101) diffraction crystallographic carbon planes for the obtained sample of CW and TNCSE, revealing the formation of carbon sheet with high graphitization. Furthermore, no other characteristic peaks in the TNCSE sample can be discovered, showing that the natural wood sheet gradually transformed from lignin to graphitized carbon during the pyrolysis process. Compared to the CW, which is not activated, the XRD patterns of TNCSE exhibit a narrower peak width, suggesting that the activation treatment further intensifies the graphitization of the electrode, which would be more beneficial in improving the conductivity of the electrode. Furthermore, TNCSE displays the (100) crystal plane with the characteristic peak shifted to the left after activation, which means that the C-edge is sliced during the activation process, forming numerous edges defects of carbon on the surface of the pore wall [41], which is consistent with the results of the Raman spectra.

Electrochemical activity markedly affects the performance of ZAB on account of the slow kinetics of the four-electron transfer reaction during the charging process. To gain insights into the advantage of self-supported TNCSE with a unique 3D structure, we carried out electrochemical tests using a standard three-electrode method and compared it with CW and powder TNCSE. OER performances of different samples are recorded in 1.0 mol/L KOH electrolyte. Fig. 5a presents the LSV curves for the OER tests of CW and TNCSE. TNCSE displays superior OER activity, with only 276 mV overpotential required to drive a current density of 10 mA/cm$^2$. In contrast, the CW has the overpotential of 450 mV at the current density of 10 mA/cm$^2$, which is much higher than that of the TNCSE. As a result, the TNCSE is found to have a higher OER activity. To further explore the effect of pore structure in electrocatalytic reactions, the TNCSE is ground into powders and loaded on the surface of carbon paper to form a powder TNCSE. As grinding to powder dramatically destroyed the 3D hierarchical structure of the carbon sheet itself, the electrocatalytic performance of the catalyst prepared from the Powder TNCSE is much lower than that of the self-supported TNCSE. Powder TNCSE loaded on carbon paper required 546 mV of voltage to drive a current density of 10 mA/cm$^2$, which is much higher than that of TNCSE derived from the natural wood (Fig. 5c). As a result, the nitrogen-doped robust carbon sheet electrode with a three-dimensional pore structure demonstrated faster OER reaction kinetics. Furthermore, the Tafel slope derived from the Tafel equation is commonly used to elucidate the rapidity of the reaction of the OER kinetic process of electrocatalysts. As illustrated in Figs. 5b and d, the Tafle slope of the TNCSE (200 mV/dec) is lower than that of the CW (490 mV/dec) and the Powder TNCSE (218 mV/dec). The superior OER catalytic activity could be attributed to the binder-free self-supported TNCSE maintaining the unique vertically hierarchical structure, which dramatically improves the electron/mass transfer with high accessibility of active sites and eventually enhances the electrochemical reaction rate.

The rechargeable zinc-air batteries are assembled and measured using the self-supported TNCSE as an air cathode. Meanwhile, TNCSE is ground to powder and loaded on carbon paper which is used as a control experiment for comparison. A rechargeable zinc-air battery is illustrated in Fig. 6a. The negative electrode consists of zinc sheets, the positive electrode is made up of different homemade samples, and the electrolyte is 6 mol/L KOH. During discharge of the battery, the cathode electrode consumes oxygen, which means that the reaction can be continued in theory if the oxygen delivery has not been interrupted. At the same time, the anode electrode consumes zinc during the discharge process so that the battery can be continuously discharged by constantly replacing the zinc. In practical Zn-air battery applications, the derived power density of ZAB assembled with Powder TNCSE as the cathode catalysts tended to increase and then decrease with increasing catalysts loading (the optimum power density was 70.91 mW/cm$^2$) (Fig. 6b). Most interestingly, the peak power density of ZAB assembled with Powder TNCSE sample of 2 mg/cm$^2$ catalysts loading is much lower than that of battery assembled with TNCSE (the peak power density was 134.02 mW/cm$^2$) having a three-dimensional structure (Fig. 6c). Since the natural three-dimensional channels have been destroyed by grounding for the Powder TNCSE sample, the electron/mass transfer would be significantly affected. In addition, charge/discharge polarization is tested on ZAB assembled with different samples, as shown in Fig. 6d. TNCSE has a low

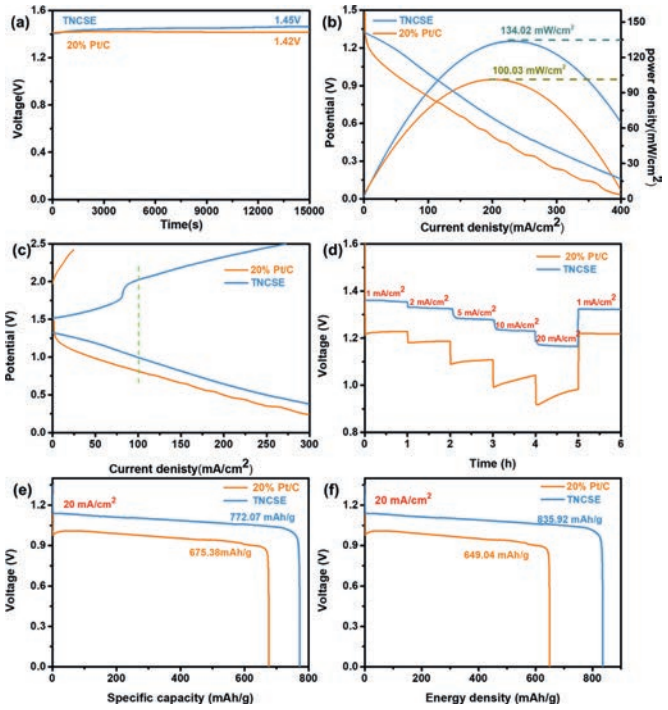


**Fig. 7.** (a) Open-circuit voltages of ZAB assembled with TNCSE and 20% Pt/C. (b, c) Power density plots and charge/discharge polarization plots. (d) Multiplicative performance curves. (e, f) Specific capacity and energy density curves.

charge/discharge voltage gap, which is much smaller than that of the battery assembled with powder TNCSE, reflecting the excellent electrochemical rechargeability of TNCSE. On the Contrary, the charging performance of a battery of powder TNCSE sample is almost down to zero. The superior performance of the TNCSE battery can be attributed mainly to the advantages of its 3D graded porous structure: (1) The 3D hierarchical porous structure provides a larger specific surface area, a higher porosity, and an exposure of a larger number of reactive sites; (2) The structure with an open and ordered array ensures easy access to the electrolyte and a fast mass transfer process, speeding up the oxygen reaction process [26]; (3) The high graphitization improves the chemical resistance of the carbon-based catalyst; (4) The stable gas-liquid-solid three-phase interface can facilitate the adsorption-dissociation of reactants and the transfer of electrons. Proper hydrophobicity can facilitate electron transfer and diffusion of oxygen reactants, providing sufficient oxygen species and reducing concentration polarization [29].

In order to explore the catalytic effect of three-dimensional hierarchical porous structures as integrated air cathodes, the ZAB with different cathode electrodes (TNCSE and 20% Pt/C catalysts loaded on carbon paper) are fabricated for comparison. The open-circuit voltage of the ZAB assembled with TNCSE is 1.45 V (Fig. 7a), which is slightly higher than 20% Pt/C catalysts (1.42 V), suggesting that TNCSE acquire much more active sites with abundant three-phase boundary and achieve the higher catalytic activity. Both of the battery's OCV does not decay during 15000 s of standing. The power density of ZAB assembled with TNCSE sample is 134.02 mW/cm$^2$, which is higher than that of battery with 20% Pt/C catalysts (100.03 mW/cm$^2$) (Fig. 7b). It can be seen in Fig. 7c that ZAB assembled with self-supported TNCSE has a much lower charge/discharge voltage gap than that of battery with 20% Pt/C catalysts, which demonstrates that ZAB assembled with TNCSE has a better electrochemical rechargeability performance. Fig. 7d indicates that ZAB assembled with the TNCSE sample has a promising multiplicative performance by conducting discharge tests at different current densities. Throughout the discharge tests at different current densities from 1 mA/cm$^2$ to 20 mA/cm$^2$, ZAB with TNCSE is able to discharge consistently. After the current density shifted from 20 mA/cm$^2$ to 1 mA/cm$^2$, the discharge potential of the battery recovered to the initial voltage stage simultaneously. After high current density discharge, the battery can still achieve voltage retention of 97.6% at low current densities, demonstrating that ZAB assembled with TNCSE has an excellent discharge multiplier performance and good reversibility. In addition, Figs. 7e and f show that ZAB with TNCSE achieves a high specific capacity of 772.07 mAh/g and an energy density of 835.92 mAh/g in a continuous discharge measurement at the current density of 20 mA/cm$^2$, which are both superior to the performance of 20% Pt/C catalysts under the same test conditions (specific capacity of 675.38 mAh/g and energy density of 649.04 mAh/g).

To further investigate the advantage of the self-supported TNCSE sample, the feature of breathable cathode structure of the Zn-air cell is diagrammed in Fig. 8a. After carbonization and activation, the well-organized and unbroken natural channels have been well preserved for the TNCSE sample, showing a well-established interface for gas-liquid-solid three-phase reactions. Natural micropore channels with excellent openness and low tortuosity can shorten oxygen diffusion distance and accelerate the gas diffusion rate. Additionally, the nitrogen-doped active sites generated by activation are uniformly distributed on the pore walls, enabling good contact with the electrolyte to form a thin electrolyte layer. This can increase the effective area of the three-phase interface for the catalyst, oxygen and electrolyte. Significantly, the by-products from the reaction could be easily emitted from the aligned tubes, allowing smoothed charge transport and reaction. Fig. 8b describes the constant current charge/discharge test curve of ZAB assembled with TNCSE at a current density of 5 mA/cm$^2$ (20 min per cycle). In the initial, the battery is discharged at 1.28 V and charged at 1.47 V in the first charge/discharge cycle, with a charge/discharge efficiency of 87.07%. In comparison, ZAB assembled with 20% Pt/C catalysts is discharged at 1.21 V and charged at 2.23 V, with a charge/discharge efficiency of only 54.26%. Under high charging voltages, the catalyst could be subjected to oxidative corrosion, which would lead to the deactivation of the performance of the battery. After 500 h of charge/discharge cycles for TNCSE sample, there is only a slight degradation in the charge/discharge performance of the battery. Interestingly, it maintains a discharge voltage of 1.31 V and a charge voltage of 1.53 V, with a charge/discharge efficiency of 85.6%. Relative to the charge/discharge efficiency of the first charge/discharge cycle, it is only a 1.47% degradation in charge/discharge efficiency after 500 h (blue inset). In contrast, the behavior of the battery with the 20% Pt/C catalyst deteriorates dramatically after only 5 h under the same test conditions (red inset). At this point, the battery was discharged at 1.06 V and charged at 1.58 V, with a charge/discharge efficiency of just 41.09%. Consequently, the zinc-air batteries assembled with TNCSE have excellent charge/discharge stability. As known from Fig. 7a, the open-circuit voltage of the ZAB assembled with TNCSE is 1.45 V, demonstrating a relatively benign catalytic performance of the TNCSE sample in practical applications. Fig. 8c shows a lamp sign "GDUT" assembled by 58 LEDs (2 V light-emitting diodes) that can be lighted by connecting two zinc-air batteries in series with no noticeable changing of brightness over a long period. To widen the application scope for our TNCSE, we adopted the TNCSE as cathode and anode in the overall water splitting device (Figs. 8d and e). As shown from Fig. 8e, a large amount of hydrogen ($H_2$) and oxygen ($O_2$) continuously appears and escapes from the surface of the TNCSE, illustrating the potential application of TNCSE in ZAB and overall water splitting in an alkaline environment.

In summary, a self-supported, robust, and porous N-dopped carbon sheet, TNCSE, was successfully developed by pyrolysis and ac-

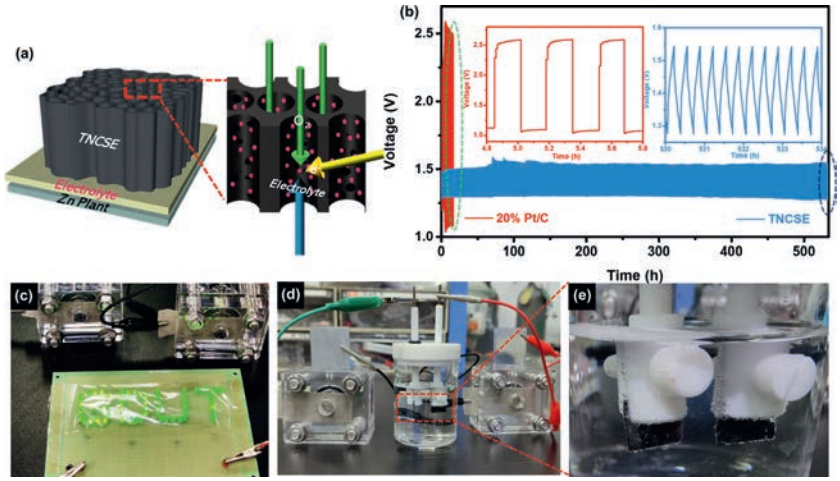


**Fig. 8.** (a) Mechanistic diagram of the ZAB breathable carbonized cathode. (b) Charge/discharge stability test curves of ZAB assembled with TNCSE and 20% Pt/C. (c) Photo of lighting LED billboard by two ZBAs in series. (d, e) Photograph of the ZAB assembled with TNCSE driving an overall water splitting device with TNCSE as cathode and anode.

tivation of pine wood. Due to the removal of cellulose and lignin from the raw timber, substantial hierarchical nanopores are produced in the walls of the macropores, allowing full exposure of the catalytic active center to the triple-phase boundary and facilitated diffusion of oxygen ions in the air cathode. Besides, nitrogen was successfully doped into the carbon skeleton with the activation treatment to generate much more active sites, which substantially improved the electrochemical activity of the obtained electrode. Most importantly, the porous microchannels of the carbon skeleton in TNCSE not only allow for the rapid transport of $Zn^{2+}$ but also for the formation of a three-phase reaction interface on the porous walls of the microchannels, enabling the catalyst to exhibit excellent cell performance with improved mass transfer in alkaline electrolytes. The ZAB with TNCSE cathode achieves a peak power density of 134.02 mW/cm$^2$ and reaches a continuous charge/discharge of 500 h, which offers a facial and cost-effective approach to develop a self-supported cathode material for Zn-air battery.

## Declaration of competing interest

There are no conflicts to declare.

## Acknowledgments

We gratefully acknowledge the financial support from the National Natural Science Foundation of China (No. 21905055), the start-up funding of Guangdong University of Technology (Nos. 220413207 and 220418129), and support from Research Fund Program of Key Laboratory of Fuel Cell Technology of Guangdong Province.

## Supplementary materials

Supplementary material associated with this article can be found, in the online version, at doi:10.1016/j.cclet.2022.03.112.

## References

[1] H.F. Wang, C. Tang, Q. Zhang, Adv. Funct. Mater. 28 (2018) 1803329.
[2] Y.P. Deng, R.L. Liang, G.P. Jiang, et al., ACS Energy Lett. 5 (2020) 1665–1675.
[3] Y.H. Tian, X.Z. Liu, L. Xu, et al., Adv. Funct. Mater. 31 (2021) 2101239.
[4] X. Lang, Z. Hu, C. Wang, Chin. Chem. Lett. 32 (2021) 999–1009.
[5] H. Liu, Q. Liu, Y. Wang, et al., Chin. Chem. Lett. 34 (2023) 107222.
[6] Q.C. Wang, X.X. Xue, Y.P. Lei, et al., Small 16 (2020) 2001571.
[7] Y.T. Zhong, Z.H. Pan, X.S. Wang, et al., Adv. Sci. 6 (2019) 1802243.
[8] H. Zhang, Z. Yang, X.M. Wang, et al., Nanoscale 11 (2019) 17384–17395.
[9] D.C. Nguyen, D.T. Tran, T.L.L. Doan, et al., Adv. Energy Mater. 10 (2020) 1903289.
[10] Z. Xu, W. Deng, X. Wang, Electrochem. Energy Rev. 4 (2021) 269–335.
[11] S. Zhang, M. Chen, X. Zhao, et al., Electrochem. Energy Rev. 4 (2021) 336–381.
[12] X. Luo, S. Chen, T. Hu, Y. Chen, F. Li, SusMat 1 (2021) 211–240.
[13] X.W. Chen, J.X. Gao, S. Liu, et al., J. Alloy Compd. 828 (2020) 154435.
[14] X.B. Zhang, X. Han, Z. Jiang, et al., Nano Energy 71 (2020) 104547.
[15] H.S. Shang, W.M. Sun, R. Sui, et al., Nano Lett. 20 (2020) 5443–5450.
[16] H. Su, W.L. Zhou, H. Zhang, et al., J. Am. Chem. Soc. 142 (2020) 12306–12313.
[17] M. Wu, G. Zhang, Y. Hu, et al., Carbon Energy 3 (2021) 176–187.
[18] J.J. Liu, T. He, Q.C. Wang, et al., J. Mater. Chem. A 7 (2019) 12451–12456.
[19] X. Liu, L. Wang, P. Yu, et al., Angew. Chem. Int. Ed. 57 (2018) 16166–16170.
[20] R.P. Zhao, Q.H. Li, Z.J. Chen, et al., Carbon 164 (2020) 398–406.
[21] Q.X. Lai, J. Zheng, Z.M. Tang, et al., Angew. Chem. Int. Ed. 59 (2020) 11999–12006.
[22] J.M. Qian, T.T. Wang, Z.M. Zhang, et al., Nano Energy 74 (2020) 104948.
[23] Z.H. Zhao, M.T. Li, L.P. Zhang, L.M. Dai, Z.H. Xia, Adv. Mater. 27 (2015) 1503211.
[24] A. Samanta, C.R. Raj, J. Power Sources 455 (2020) 227975.
[25] H.B. Yang, J. Miao, S.F. Hung, et al., Sci. Adv. 2 (2016) e1501122.
[26] D. Dang, R.J. Zeng, X.W. Chen, et al., Catal. Commun. 159 (2021) 106351.
[27] J. Yu, B.Q. Li, C.X. Zhao, J.N. Liu, Q. Zhang, Adv. Mater. 32 (2020) 1908488.
[28] Q.Z. Zhang, M.H. Zhou, G.B. Ren, et al., Nat. Commun. 11 (2020) 1731.
[29] X. Liu, G.Y. Zhang, L. Wang, H.G. Fu, Small (2021) 2006766.
[30] L.L. Du, X. Luo, F.Y. Zhao, et al., Carbon 96 (2016) 685–694.
[31] L. Du, L.X. Xing, G.X. Zhang, S.H. Sun, Carbon 156 (2020) 77–92.
[32] Y.H. He, H. Guo, S. Hwang, et al., Adv. Mater. 32 (2020) 2003577.
[33] A.R. Koltonow, J.X. Huang, Science 351 (2016) 1395–1396.
[34] X. Liu, L.M. Dai, Nat. Rev. Mater. 1 (2016) 16064.
[35] H.Y. Song, S.M. Xu, Y.J. Li, et al., Adv. Energy Mater. 8 (2018) 1701203.
[36] X.W. Peng, L. Zhang, Z.X. Chen, et al., Adv. Mater. 31 (2019) 1900341.
[37] H.L. Zhu, W. Luo, P.N. Ciesielski, et al., Chem. Rev. 116 (2016) 9305–9374.
[38] J. Garemark, X. Yang, X. Sheng, et al., ACS Nano 14 (2020) 7111–7120.
[39] F. Jiang, T. Li, Y.J. Li, et al., Adv. Mater. 30 (2018) 1703453.
[40] D. Luo, X.Q. Zhang, J. Hydrogen Energy 43 (2018) 5668–5679.
[41] L.Q. Wang, K.X. Liang, L. Deng, Y.N. Liu, Appl. Catal. B: Environ. 246 (2019) 89–99.